ACS APPLIED MATERIALS & INTERFACES

www.acsami.org Research Article

Insights into the Mechanism of the Mechanochemical Formation of Metastable Phases

Resham Rana, Daniel Long, Paul Kotula, Yufu Xu, Dustin Olson, Jules Galipaud, Thierry LeMogne, and Wilfred T. Tysoe*

Cite This: *ACS Appl. Mater. Interfaces* 2021, 13, 6785–6794 Read Online

ACCESS | Metrics & More | Article Recommendations | Supporting Information

ABSTRACT: The mechanochemical reaction kinetics of sulfur with copper to form a metastable copper sulfide phase at room temperature is investigated in ultrahigh vacuum by modifying the properties of the copper during cleaning in vacuum. The measured kinetics is in agreement with a theory first proposed by Karthikeyan and Rigney that predicts that the rate depends linearly both on the contact time and on the strain-rate sensitivity of the substrate. The mechanism for this process was investigated using thin samples of copper fabricated using a focused-ion-beam and by measuring the crystal structure and elemental composition of the copper subsurface region by electron microscopy after reaction. The measured sulfur depth distributions produced by shear-induced surface-to-bulk transport were in good agreement with values calculated using rate constants that also model the reaction kinetics. Sulfur was found both in crystalline regions and also concentrated along grain boundaries, implying that formation of metastable phases is facilitated by both the presence of dislocations and by grain boundaries.

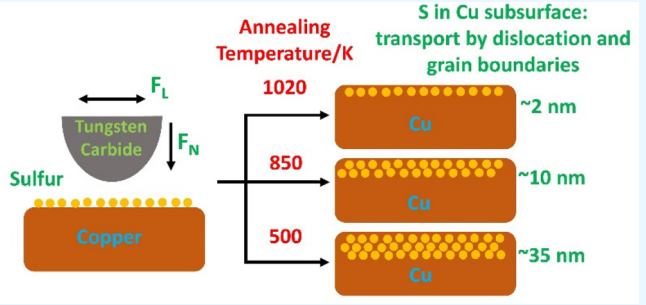

KEYWORDS: *dialkyl sulfide, copper, shear-induced surface-bulk transport kinetics, Auger spectroscopy, electron microscopy, focused-ion-beam samples*

INTRODUCTION

Mechanochemical processes often initiate novel and "green" solid-state reactions that can result in the formation of metastable materials that are not accessible through thermal processes.[3−9] Mechanochemical reactions can be induced at ambient temperatures and do not generally require a solvent. Such solid-state reactions have been known for millennia; the mechanical reduction of cinnabar to mercury in a copper pestle and mortar was reported in ∼315 BC[10] and Faraday studied the mechanochemistry of solids in the 19th century.[11] However, little is known about the mechanism by which such metastable materials are formed, although it has been suggested that they are caused either by energy dissipation at collision sites that increases local temperatures, through the formation of defect sites,[12−15] or by dislocation glide.[16−18] Significant structural changes have also been found for sheared metals; copper forms nanocrystalline structures in the subsurface region.[19−25]

This issue is addressed using the mechanochemical reaction between dimethyl disulfide (DMDS) and copper in ultrahigh vacuum. In the absence of an external force, DMDS and copper react stoichiometrically via S—S bond scission to form adsorbed methyl thiolate species, which are thermally stable at room temperature, and the reaction ceases at this step. Two distinct mechanochemical processes are induced by rubbing the copper with a tungsten carbide ball in the presence of DMDS. First is the decomposition of the adsorbed methyl thiolate species to evolve gas-phase hydrocarbons and deposit atomic sulfur on the surface.[2,26−29] The second process, relevant to the mechanochemical synthesis of novel materials, is the shear-induced surface-to-bulk transport of the adsorbed sulfur to produce a metastable CuS_x phase. Note that the sliding conditions during these experiments are sufficiently mild so that the temperature rise is negligible (≪1 K).[1] Here, the adsorbed sulfur formed by methyl thiolate decomposition is lost from the surface to create new sites that allow the reaction to continue. The metastability of the sulfide phase was demonstrated by showing that the subsurface sulfur thermally diffused to the surface once again on heating to a high temperature.[1,2]

The first-order rate constants for these elementary-step reactions have been measured and used to construct a kinetic model that predicts the mechanochemical reaction kinetics, the

Received: October 22, 2020
Accepted: January 25, 2021
Published: January 28, 2021

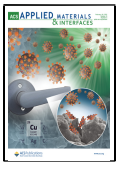

https://dx.doi.org/10.1021/acsami.0c18980
ACS Appl. Mater. Interfaces 2021, 13, 6785–6794

evolution in friction as a function of the number of passes, the depth profile of the sulfur in the copper bulk, and the variation in the total amount of subsurface sulfur.[2] Note that the reaction could be viewed as either a mechanocatalytic reaction or a tribochemical process depending on whether the focus is on the formation of gas-phase products or the deposition of a friction-reducing film.[30]

The kinetic analysis assumed that the distance that a sulfur overlayer diffuses into the copper is proportional to the number of times that it had been rubbed to produce an effectively first-order rate constant.[29] This agrees with molecular dynamics (MD) simulations of sliding interfaces which reveal the formation of shear-induced vortices that cause surface atoms to be transported into the bulk.[31,32] The resulting patterns formed in the near-surface region of the sample resemble those produced in shear by classical Kelvin–Helmholtz (K-H) instabilities despite the differences in effective viscosity values,[33−38] resulting in subsurface copper structures that can lead to surprisingly low friction.[6,39,40]

An analytical model for these phenomena proposed by Karthikeyan and Rigney (KR)[41] assumes a material flow law given by the Herschel-Bulkley equation, where the shear stress $\tau_{xy} = \tau_0 + C\left(\frac{du}{dy}\right)^m$[42] and τ_0 and C are fitting parameters, m is the strain-rate sensitivity that can take values between 0 and 1, and $\frac{du}{dy}$ is the shear strain rate. The KR model predicts that the time dependence of the characteristic width of the deformed zone, y^*, depends on the value of m. Since metals and, in particular copper, have $m \ll 1$,[43,44] this leads to $y^* \propto t$ (see below). Since the contact time is proportional to the number of passes p at a constant sliding speed and load, this prediction is in accord with experiment.

As demonstrated below, the value of y^* also depends linearly on the strain-rate sensitivity, m, which, for metals in general, and for copper in particular, decreases with the size of the nanocrystallites[5,23,43−48] The initial crystallite size in turn depends on the temperature at which the copper had been annealed during cleaning (see Experimental section), and if the crystallites formed during rubbing depend on the initial crystallite sizes, the surface-to-bulk transport kinetics will also depend on the initial crystallite size. Since the hardness is a gauge of crystallite size through the Hall-Petch effect,[49,50] this suggests that the rate of metastable sulfide phase formation should correlate with the copper hardness. These ideas are tested by measuring the nanohardness of copper samples that had been annealed at different temperatures (500, 850, and 1020 K) during cleaning in UHV, where it is found that the hardness of the rubbed regions does depend on the initial hardness. The surface-to-bulk transport rate is shown to vary linearly with strain-rate sensitivity and the mechanism is investigated by studying the depth profile of focused-ion-beam (FIB) prepared samples that had been rubbed in the presence of DMDS to identify whether the sulfur was located at the interface between grains (in which case, the transport is grain-boundary mediated) or uniformly distributed throughout the sample (in which case, the mechanically induced transport kinetics are mediated by dislocations).

METHODS

Experiments were carried out in a stainless-steel, ultrahigh vacuum (UHV) chamber operating at a base pressure of ~2 × 10^{-10} Torr following bakeout, which has been described in detail elsewhere.[51] Briefly, the chamber was equipped with a UHV-compatible tribometer, which simultaneously measures normal load, lateral force, and the electrical contact resistance between the tip and substrate. All measurements were made using a sliding speed of ~4 mm/s at a normal load of 0.44 N. Previous work has shown that the maximum interfacial temperature rise for a copper sample under these conditions is much less than 1 K.[1] The spherical pin (~12.7 mm diameter) was made from tungsten carbide containing some cobalt binder and could be heated by electron bombardment *in vacuo* or by argon ion bombardment in order to clean it. The pin was mounted onto an arm with attached strain gauges to enable the normal and lateral forces to be measured. The arm was mounted to a rotatable Conflat flange to allow the pin to be rotated to face a cylindrical-mirror analyzer (CMA) to enable Auger spectra of the pin surface to be obtained. Additional experiments were carried out by analyzing the tungsten carbide pin by X-ray photoelectron spectroscopy (XPS) after argon ion bombardment using a spectrometer containing a hemispherical analyzer built by ThermoFisher (220i) with a focused Al Kα monochromatic X-ray source.

The copper samples (Alfa Aesar, 99.99% pure, 1 mm thick) were polished to a mirror finish using 1 μm diamond paste and then rinsed with deionized water and degreased ultrasonically in acetone before mounting in the UHV chamber. The copper was cleaned using a standard procedure which consisted of argon ion bombardment (~1 keV, ~2 μA/cm^2) and annealing cycles of ~10 min to ~500, 850, or 1020 K to result in different crystallite sizes and mechanical properties. The argon ion bombardment and annealing cycles were repeated until the copper samples were clean, and cleanliness of the samples was monitored using Auger spectroscopy.

The samples were mounted in UHV either to a precision x, y, z manipulator for measuring the sulfur concentration across a rubbed region of the sample or to a transfer arm that allowed the sample to be moved from the UHV chamber to a small cell which could be isolated by a gate valve from the main chamber.[52] The transfer arm slid through a differentially pumped seal and the copper could be resistively heated with the temperature measured via a thermocouple. A 1 μm thick film of aluminum could be deposited on the copper when enclosed in the cell to protect it from atmospheric contamination during transport to Sandia National Laboratories for additional analysis.

The tribometer chamber contained a single-pass CMA for Auger analysis and an argon ion bombardment source for sample cleaning and depth profiling. Auger spectra were either collected using the coaxial electron gun in the CMA using an electron beam energy of 3 kV or with a Staib model EK050M2 Microfocus electron gun. The chamber is also equipped with a channeltron secondary electron detector which allowed scanning electron microscopy (SEM) images of the wear scar to be collected using the microfocus electron gun. Auger elemental profiles across the rubbed regions were obtained to measure the loss of sulfur from the surface as a function of the number of times that the sample had been rubbed. To ensure that the sulfur signal was being measured only in the rubbed region and did not include signals from the unrubbed part of the sample, calibration experiments were carried out to focus the electron beam on a 100 μm diameter silver wire and by detecting Auger signals due only to silver. Concentration profiles across the rubbed region were measured either by moving the sample laterally by translating the precision manipulator to which the copper sample was mounted, or by deflecting the electron beam by using capacitor plates incorporated in the high-resolution electron gun. Both methods yielded identical results for the variation in Auger signal as a function of the number of times that it had been rubbed. Finally, the chamber also included a quadrupole mass spectrometer for leak checking and for gauging reactant purity. Nanoindentation measurements were made using a Nanoindenter G200 (KLA/Agilent) with an ~130 nm Berkovich tip.

All experiments were performed by initially rubbing the pin against the clean copper sample (~1.7 × 1.7 cm^2 by ~1 mm thick) until a constant friction coefficient (μ = ~0.53)[27] was obtained. This resulted in the formation of a wear track that attained a constant width after the friction became constant, so that wear was assumed to have

https://dx.doi.org/10.1021/acsami.0c18980
ACS Appl. Mater. Interfaces 2021, 13, 6785−6794

ceased. DMDS was dosed through a leak valve connected to a dosing tube (with an internal diameter of 4×10^{-3} m) directed toward the sample so that the pressure at the sample is enhanced compared to the background pressure, which was set at 1×10^{-8} Torr during DMDS dosing (pressures are not corrected for ionization gauge sensitivity).

In the first experiment, the loss of sulfur from a saturated methyl thiolate overlayer formed by dosing the rubbed sample with DMDS was measured by Auger spectroscopy as a function of the number of times that it had been rubbed for samples that had been cleaned by annealing to 500, 850, or 1020 K.

In a second experiment, samples were prepared by rubbing copper samples that had been annealed at 500, 850, or 1020 K in a background pressure of 5×10^{-8} Torr of DMDS for 80 cycles at a load of 0.44 N to cause sulfur to react with the copper. The sulfur depth distribution has been measured previously by angle-resolved XPS, which also showed that the bulk sulfur concentration was relatively low and not likely to influence the mechanical properties of the copper.[2] This protocol provided higher subsurface sulfur concentrations for subsequent *ex situ* analyses at Sandia National Laboratories. Electron-transparent lamella ($11\ \mu m \times 6.7\ \mu m \times 16\ \mu m$ deep) were prepared from these aluminum-coated copper samples at the Center for Integrated Nanotechnologies (CINT) at Sandia National Laboratories using a Thermo Scientific Scios 2 DualBeam focused-ion beam (FIB) apparatus. Scanning transmission electron microscopy (STEM) and energy dispersive X-ray spectroscopy (EDXS) were done with a FEI (now Thermo Fisher Scientific) Titan G2 80-200 electron microscope equipped with a spherical aberration corrector on the probe-forming optics, and four silicon-drift X-ray detectors operating at 200 kV electron energy.

The DMDS (Aldrich, 99.0% purity) was transferred to a glass bottle and attached to the gas-handling system of the vacuum chamber, where it was subjected to several freeze−pump−thaw cycles. The purity of the DMDS was monitored using mass spectroscopy.

Modified Karthikeyan−Rigney (KR) Model for Interfacial Mixing at a Sliding Interface. The following outlines a modification of the analysis by Karthikeyan−Rigney[41] for the mixing at a sliding interface to specifically investigate the dependence on strain-rate sensitivity. The model assumes that the flow properties of copper are described by the Herschel−Bulkley model[42] where

$$\tau_{xy} = \tau_0 + C\left(\frac{du}{dy}\right)^m \tag{1}$$

Writing $u(y,t) = U(\lambda)$ where $\lambda = yt^{\alpha}$, and $\alpha = -\frac{1}{m+1}$, the Cauchy equation of motion gives the following differential equation for the velocity $U(\lambda)$

$$\lambda\left(\frac{dU}{d\lambda}\right)^{2-m} = -\left(\frac{Cm(1+m)}{\rho}\right)\frac{d^2U}{d\lambda^2} \tag{2}$$

where ρ is the density. We derive a solution for the case in which $m \ll 1$, typical of a metal such as copper,[21,44,45,53] so that $\lambda = yt^{-1}$ and eq 2 simplifies to

$$\lambda\left(\frac{dU}{d\lambda}\right)^{2} = -\left(\frac{Cm}{\rho}\right)\frac{d^2U}{d\lambda^2} \tag{3}$$

A general solution of this equation is

$$U(\lambda) = c_2 - \sqrt{\frac{2A}{c_1}}\arctan\left(\frac{\lambda}{\sqrt{2Ac_1}}\right) \tag{4}$$

where $A = \frac{Cm}{\rho}$ and c_1 and c_2 are constants of integration, which are determined from the boundary conditions. Using the no-slip KR boundary conditions[41] which, at $\lambda = 0$, gives $U(0) = 0$, so that $c_2 = 0$, and at $\pm\infty$, gives $U(\pm\infty) = \pm U$ and $\frac{dU(\lambda)}{d\lambda} = 0$. The second condition is automatically obeyed from the form of the function in eq 4. Applying the first boundary condition yields

$$\sqrt{\frac{2A}{c_1}} = -\frac{2U}{\pi} \tag{5}$$

where $\sqrt{2Ac_1} = \frac{\pi A}{U} = \frac{C\pi m}{\rho U} \equiv B$, to give the full solution as

$$U(\lambda) = \frac{2U}{\pi}\arctan\left(\frac{\lambda}{B}\right) \tag{6}$$

However, the sliding conditions for copper in the experiments carried out in this work involve a stationary copper substrate and a pin sliding at a velocity U. This now gives boundary conditions; at $\lambda = 0$, $U(0) = U$, and at $+\infty$, $U = 0$ and $\frac{dU(\lambda)}{d\lambda} = 0$, so that now

$$U(\lambda) = U - \frac{2U}{\pi}\arctan\left(\frac{\lambda}{B}\right) \tag{7}$$

The slope at the origin is given by

$$\left.\frac{dU}{d\lambda}\right|_{\lambda=0} = -\frac{2U}{\pi B} \tag{8}$$

Taking the average value of λ^* to be that at which the linear extrapolation of $U(\lambda)$ becomes zero gives

$$1 - \frac{2U}{\pi B}\lambda^* = 0 \tag{9}$$

Substituting $\lambda^* = \frac{y^*}{t}$ gives $y^* \propto mt$ and predicts that the surface layer moves at a constant distance per pass as found experimentally[1,2,27,29,54,55] and that this distance is proportional to the strain-rate sensitivity, m. Since the strain-rate sensitivity and hardness depend on crystallite size,[56] the hardness values of the copper samples are measured after heating to various temperatures to control the crystallite size, and the results correlated with the surface-to-bulk transport kinetics of sulfur to form a metastable CuS_x phase.

RESULTS AND DISCUSSION

The dependence of the copper crystallite size on annealing temperature is illustrated in the Supporting Information (Figure S1a−c); the resulting nanohardness values were measured on the rubbed and unrubbed areas of the samples and are shown in the Supporting Information (Figures S2 and S3). This indicates that the hardness in the rubbed region does depend on the cleaning temperature thereby confirming that samples with different initial mechanical properties can be obtained by varying the temperature at which the sample was heated. However, the elastic moduli were found to be the independent of annealing temperature (Figure S4). The analysis of tungsten carbide tribopin is shown in Figure S5.

Measurement of the Kinetics of Sulfur Surface-to-Bulk Transport in Copper as a Function of Sample Annealing Temperature. The rates of surface-to-bulk transport were measured for copper samples that had been annealed at 500, 850, or 1020 K during their preparation. The sulfur coverage was measured as a function of position across the rubbed region (wear track) by Auger spectroscopy using a small-spot-size electron gun.[55] The signal includes contributions from the methyl thiolate overlayer and adsorbed sulfur as well as subsurface sulfur.[29] Disentangling these contributions requires the rate of shear-induced methyl thiolate decomposition to be measured from the methane formed during sliding.[55] The surface was dosed with DMDS at a sample temperature of 300 K to form a saturated methyl thiolate overlayer[57] and the coverages were measured by monitoring the S KLL Auger signal at 151 eV kinetic energy. Full Auger spectra were collected within the wear track and the sulfur coverage was gauged from the ratio of the peak-to-peak

https://dx.doi.org/10.1021/acsami.0c18980
ACS Appl. Mater. Interfaces 2021, 13, 6785−6794

intensities of the S KLL to the Cu LMM Auger features. The surface was then rubbed, and signals were measured at various intervals until no sulfur was detected. The resulting plots of the normalized S/Cu Auger ratio as a function of the number of passes are displayed in Figure 1 for samples that had been

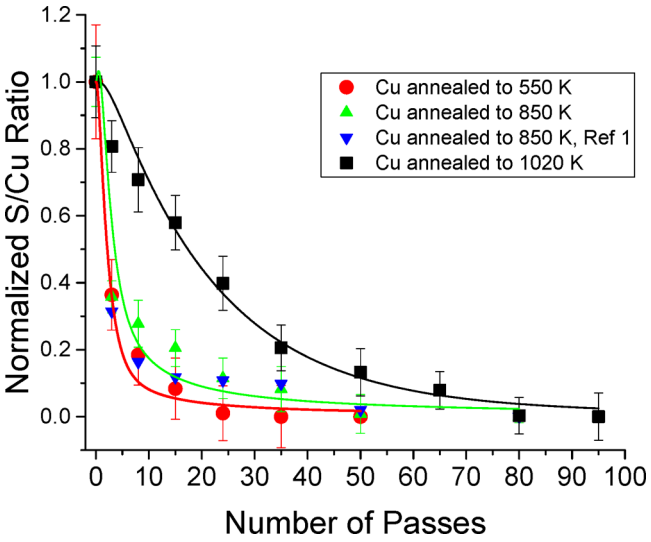

Figure 1. Surface-to-bulk transport kinetics. Plot of the relative sulfur to copper (S/Cu) Auger ratio measured inside the wear track as a function of the number of times that the copper samples had been rubbed in a background pressure of 1×10^{-8} Torr of DMDS at an applied normal load of 0.44 N and a sliding speed of 4 mm/s after being cleaned and annealed at 500 (●, red), 850 (▲, green) and 1020 (■, black) K. Shown for comparison are the results obtained previously for a sample that had been heated to 850 K (▼, blue).[1] The errors in the C/Cu Auger ratios are determined from the standard deviation of several measurements.

annealed at 500 (red circle), 850 (green triangle) or 1020 (black square) K. The experiments were repeated several times, were very reproducible, and revealed that there are significant differences in the rates at which sulfur was lost from the surface. Shown for comparison are the results obtained previously for a sample that had been heated to 850 K (blue inverted triangle),[1] where the agreement with the current results is good.

Methyl thiolate species react by two distinct shear-induced processes, the first being C—S bond scission, with a first-order rate constant k_1/s, and the second is sulfur surface-to-bulk transport with a first-order rate constant k_2/s.[2,29,58] Because the time that the tip stays in contact with a point on the surface is not precisely known, reaction rates are described as a function of the number of passes over the surface which, for sulfur surface-to-bulk transport, is denoted as k_2'/pass. The results in Figure 1 are analyzed to yield values of k_2' (per pass), and the fits are shown as solid lines though the data and the results are summarized in Table 1. The value of k_2' defines the characteristic distance that the sulfur penetrates the bulk of the sample. In the case of the experiments carried out in this work, the depth at which the sulfur concentration is predicted to decrease to ∼50% of the value at the surface for the sample annealed to ∼1020 K is very small (∼0.3 nm), increasing to ∼10 nm for a sample heated to 850 K, and ∼35 nm for a sample heated to 500 K.

Subsurface Structure and Composition of Copper as a Function of Sample Annealing Temperature. Copper samples were prepared using a similar protocol in which an initial wear track was created, and the sample then rubbed while being continuously exposed to gas-phase DMDS at a background pressure of 5×10^{-8} Torr for 80 scans. The samples were then coated with aluminum to provide a protective layer, and FIB samples were extracted from the rubbed regions and analyzed. Figure S1d,e shows high angle annular dark-field (HAADF) transmission electron microscopy (TEM) images, and Figure S1f shows an FIB scanning electron microscope (SEM) image of the subsurface regions of copper samples that had been prepared by heating to various temperatures. The results show that the measured crystallite sizes agree with those obtained from the hardness measurements (Table 1). Energy-dispersive X-ray (EDX) spectral images (comprising a full X-ray spectrum at each pixel in an array) were acquired from selected areas of each sample close to the copper surface to investigate the depth distribution and location of sulfur in the subsurface region of the sample.

Figure 2 is a 100 nm × 50 nm image of a sample that had been cleaned and annealed at 1020 K and then reacted in DMDS while rubbing showing the component distribution (the location and amount are shown in a color overlay) and the corresponding X-ray spectra, which indicate which elements are present at a particular location. The X-ray spectral image was analyzed by Sandia's Automated eXpert Spectral Image Analysis (AXSIA) software.[59,60] Thus, the component image and corresponding spectral shape matrices represent a reduced-rank and denoised model of the original spectral image. The X-ray energies are indicative of the elements present in the sample, where copper has a characteristic K_α energy at 8.040 keV, a K_β energy at 8.905 keV, and an L_α energy at 0.928 keV and is clearly evident in the Cu component spectra (red). It is uniformly distributed throughout the sample as seen in the color overlay. The dark region at the top of the image is the aluminum capping layer (component spectral shape not shown). Sulfur is clearly evident in the Cu−S spectra (green) from the K_α peak at 2.307 keV and is localized at the copper surface, consistent with the small k_2' value (Table 1). A small amount of oxygen contamination is evident in the Cu−S component from its characteristic K_α energy at 0.525 keV.

The large crystallites in the sample that had been annealed to 1020 K (Table 1) results in a low surface-to-bulk transport

Table 1. Parameters for Copper Annealed and Cleaned *In Vacuo* at Various Temperatures

annealing temperature/K	H/GPa	estimated grain size[a]/nm	measured grain size[b]/nm	h^*[c]/nm	dislocation density[d]/m^2 × 10^{13}	k_2'/pass
500	1.35 ± 0.02	115	97 ± 13	284	3.95	4 ± 1
850	1.15 ± 0.05	250	350 ± 70	465	2.4	2.5 ± 0.2
1020	0.72 ± 0.01	1400	1200 ± 120	1178	0.95	0.051 ± 0.004

[a]Values estimated from the Hall-Petch equation (eq S2). [b]Measured from electron microscope images in S1d–f. [c]Measured from the Nix-Gao formula (eq S1). [d]Estimated using eq S3 using the value of h^*.

https://dx.doi.org/10.1021/acsami.0c18980
ACS Appl. Mater. Interfaces 2021, 13, 6785−6794

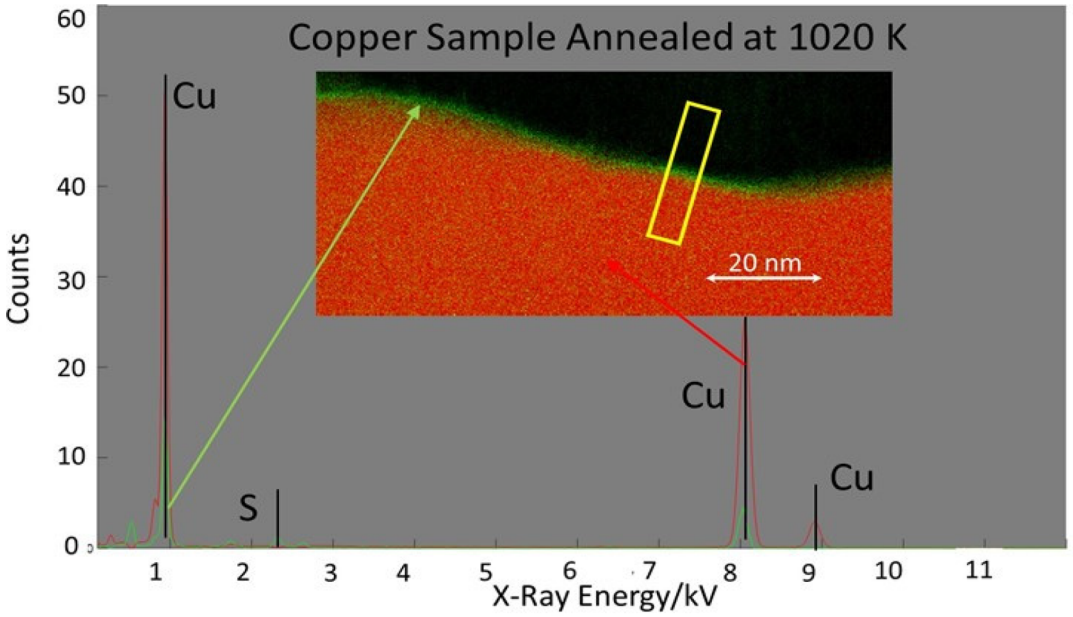

Figure 2. A 100 nm × 50 nm EDXS image of a copper foil that had been cleaned and annealed in UHV at 1020 K and then reacted while rubbing for 80 cycles at an applied normal load of 0.44 N and a sliding speed of 4 mm/s in 5×10^{-8} Torr of DMDS. The interface between the copper and the aluminum capping layer is at the top of the image and the X-ray spectra displayed for various points in the image are indicated by colored arrows.

rate (Figure 1) and a small value of k_2'. The rate constant is proportional to the distance that the sulfur moves into the subsurface region per pass, and the kinetic model for the reaction of DMDS with copper can be analyzed to yield the sulfur depth distribution as a function of the number of passes.[2] This analysis predicts that the sulfur should only penetrate a few angstroms into the subsurface of a sample annealed at 1020 K, consistent with the narrow sulfur-containing band seen in Figure 2. An integrated profile of the sulfur signal as a function of depth is displayed in Figure 3 (black square), collected from region defined by the yellow box in Figure 2, and has a width of ∼2 nm with a maximum at ∼0.5 nm below the surface. This implies that the spatial resolution of the instrumental and experimental configuration is ∼1 nm, primarily due to broadening of the electron beam (initially smaller than ∼0.12 nm) as it interacts with the sample. The solid line through the data in Figure 3 shows the theoretically predicted profile broadened by numerically convoluting it with a 1 nm wide Gaussian function using Origin software, leading to good agreement with the experimental profile.

Similar results are presented in Figure 4 for a sample that had been cleaned and annealed at 850 K and then reacted with DMDS while rubbing. Here, the average crystallite size is ∼250 nm, approximately the same as the 200 nm × 100 nm field of view of the X-ray spectral image. Again the component X-ray spectra show the presence of copper and sulfur, where the sulfur is located near the surface of the sample (indicated by the green component in the color overlay) but penetrates further into the bulk than for the sample annealed at 1020 K (Figure 3), in accord with the larger value of k_2' for a sample annealed to 850 K (Figure 1 and Table 1). Note that the analyzed region in Figure 4 consists of a single copper grain demonstrating that surface-to-bulk transport is facilitated by dislocations.[61−63]

A profile of the Cu−S EDXS signal is plotted in Figure 5 (black square) as a function of distance into the sample in the

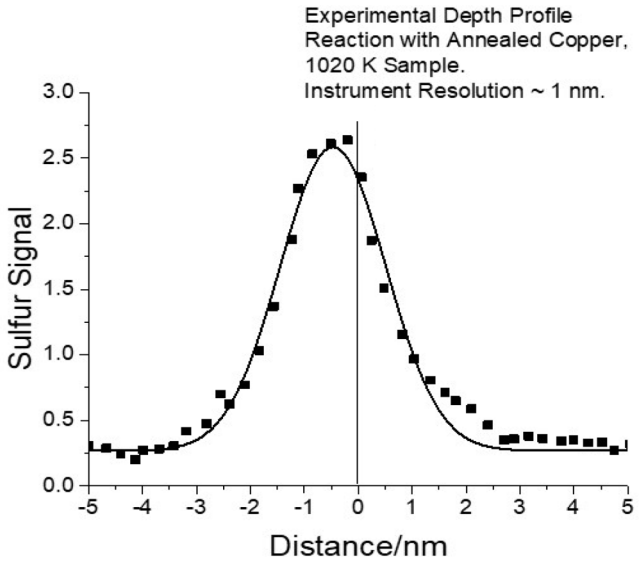

Figure 3. Plot of the intensity of the sulfur Kα X-ray signal at 2307 eV as a function of distance from the surface of a copper foil that had been cleaned and annealed in UHV at 1020 K and then reacted while rubbing for 80 cycles at an applied normal load of 0.44 N and a sliding speed of 4 mm/s in 5×10^{-8} Torr of DMDS, where the origin of the abscissa represents the surface, where negative values are within the copper sample (■). The line through the data is a fit to the theoretical depth profile[2] which has been broadened by 1 nm to take account of the spatial resolution of the instrument.

region defined by the yellow rectangle in Figure 4. Here the sulfur signal peaks at ∼4 nm below the surface but penetrates tens of nanometers into the bulk. Note that previous angle-resolved XPS results for a sample that had been annealed at 850 K and reacted in DMDS yielded profiles that were in excellent agreement with the depth profile calculated using the kinetic model described above.[2] A sulfur depth profile that was broadened by convoluting it with a 1 nm wide Gaussian

https://dx.doi.org/10.1021/acsami.0c18980
ACS Appl. Mater. Interfaces 2021, 13, 6785−6794

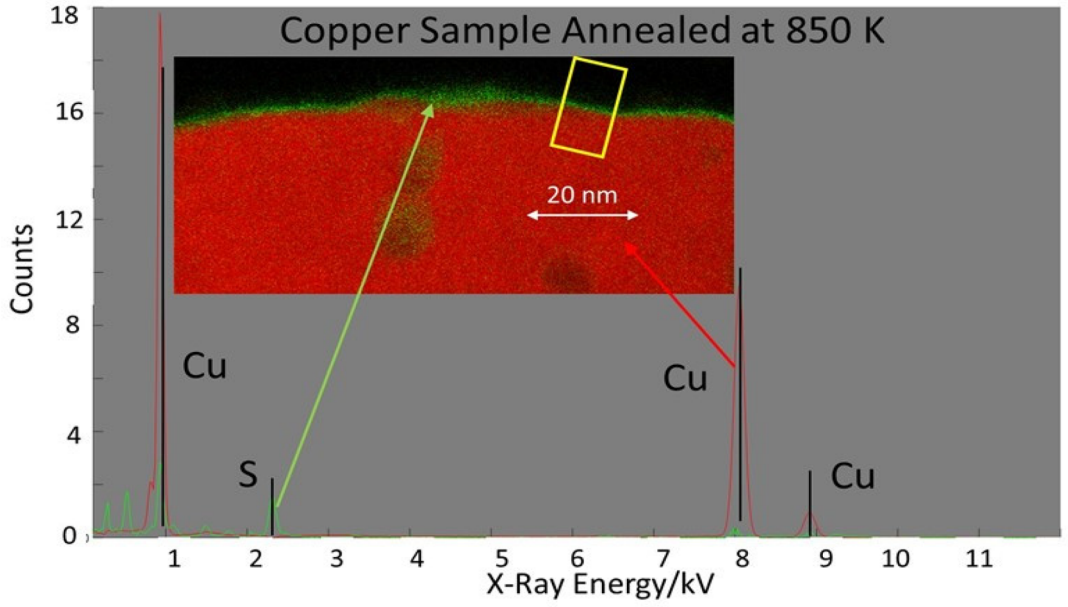

Figure 4. A 200 nm × 100 nm EDXS image of a copper foil that had been cleaned and annealed in UHV at 850 K and then reacted while rubbing for 80 cycles at an applied normal load of 0.44 N and a sliding speed of 4 mm/s in 5×10^{-8} Torr of DMDS. The interface between the copper and the aluminum capping layer is at the top of the image and the X-ray spectra displayed for various points in the image are indicated by colored arrows.

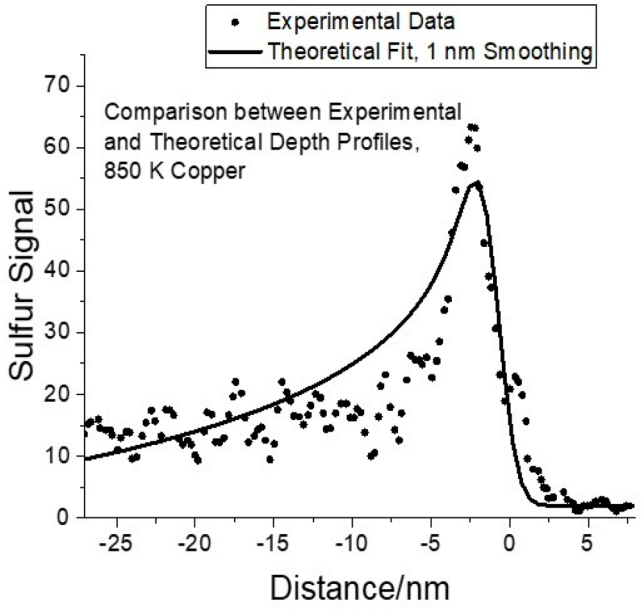

Figure 5. Plot of the intensity of the sulfur Kα X-ray signal at 2307 eV as a function of distance from the surface of a copper foil that had been cleaned and annealed in UHV at 850 K and then reacted while rubbing for 80 cycles at an applied normal load of 0.44 N and a sliding speed of 4 mm/s in 5×10^{-8} Torr of DMDS, where the origin of the abscissa represents the surface, where negative values are within the copper sample (black square). The line through the data is a fit to the theoretical profile[2] which has been broadened by 1 nm to take into account the spatial resolution of the instrument.

calculated using $k_2' = 2.5$/scan (Table 1) is plotted as a solid line in Figure 5. The agreement with the experiment is reasonable, although there are differences between theory and experiment, likely due to local concentration variations from the small sampling area. In addition, the sample surface may not be exactly parallel to the electron beam due to roughness.

A similar spectral image analysis is shown for a sample that had been cleaned and annealed at 500 K in Figure 6. Here, the field of view is 480 nm × 320 nm, while the average crystallite size of this sample is ∼100 nm (Table 1). A line is included in the image to indicate the surface. The spectral image shows a sulfur-rich region adjacent to the surface to a depth of ∼65 nm, but with less sulfur at larger depths. This region is somewhat heterogeneous and will thus yield depth profiles that will depend significantly on the measurement position. However, the depth profile calculated using $k_2' = 4.0$/scan (Table 1) is shown as an inset to the figure and indicates that the width of the subsurface sulfur-rich region agrees with the theoretically predicted profile. These results indicate that the experimental variation in the sulfur depth with sample annealing temperature agrees with the calculated depth profiles using the measured surface-to-bulk transport rate constants. In particular, the sulfur depth profile and surface-to-bulk transport rate constants correlate with dislocation densities (Table 1).

There are also linear, sulfur-rich features found deeper into the sample that are separated by ∼100 nm, close to the final grain size of the 500 K annealed copper sample. Figure S1d shows a HAADF TEM image of this sample, where the red square highlights the region analyzed in Figure 6, confirming that the sulfur-rich regions do correspond to the locations of the grain boundaries. This implies that sulfur transport along grain boundaries can also facilitate the surface-to-bulk transport of sulfur in copper.[61−63]

Modified KR theory predicts that the shear-induced rate of sulfur transport into the bulk of copper to form a metastable copper sulfide depends on (i) the strain-rate sensitivity of the substrate and (ii) is proportional to the number of times that the sample has been rubbed. The second prediction has been confirmed experimentally[55] and has been used to model the gas-phase reaction between copper by DMDS.[2]

The predicted strain-rate sensitivity dependence was tested on samples that had been cleaned and annealed at different

https://dx.doi.org/10.1021/acsami.0c18980
ACS Appl. Mater. Interfaces 2021, 13, 6785−6794

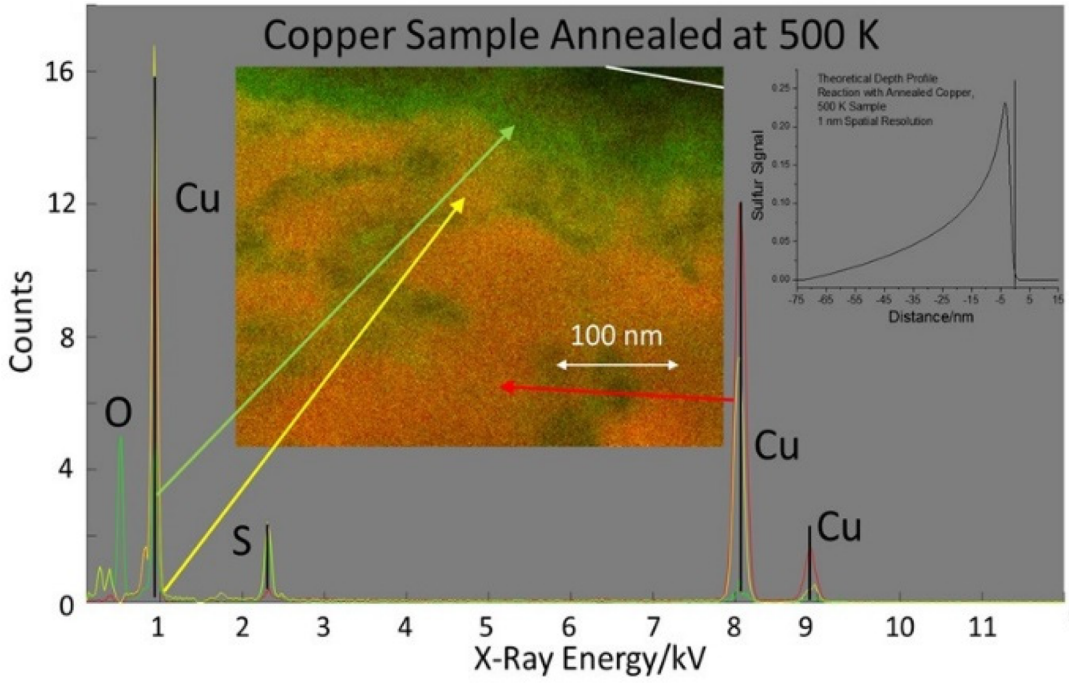

Figure 6. A 480 nm × 320 nm EDXS image of a copper foil that had been cleaned and annealed in UHV at 500 K and then reacted while rubbing for 80 cycles at an applied normal load of 0.44 N and a sliding speed of 4 mm/s in 5×10^{-8} Torr of DMDS. The interface between the copper and the aluminum capping layer is at the top of the image and is indicated by a white line, and the X-ray spectra displayed for various points in the image are indicated by colored arrows. The inset to the spectra shows the predicted depth profile[2] which has been broadened by 1 nm to take into account the spatial resolution of the instrument.

temperatures (500, 850, or 1020 K) to produce copper with different initial grain sizes (Figure S1, Table 1). Measurements of the surface-to-bulk transport kinetics yielded significantly different values of the rate constant, k_2' (Figure 1, Table 1), depending on the sample annealing temperature. Since the hardness of copper depends on grain size through the Hall–Petch effect,[56] and the strain-rate sensitivity also depends on the size of the crystallites (Figure S6, modified from ref 56),[64] the dependence of the rate of surface-to-bulk transport of sulfur into copper (k_2') on strain-rate sensitivity m is shown in Figure 7, and the linear dependence is in accord with the prediction of the model.

In order to identify the origin of the strain-rate sensitivity dependence of the rate of sulfur surface-to-bulk transport, the elemental depth distribution was measured using EDXS and the results are displayed in Figures 2, 4 and 6. For a sample that had been annealed at 1020 K (Figure 2), the sulfur is located very close to the surface (Figure 3), consistent with the measured value of $k_2' \sim 0.05$ per pass. Here, the crystallite sizes are large (~1400 nm, Table 1) and the dislocation density, obtained as indicated in Supporting Information from eq S3, is low ($\sim 9.5 \times 10^{12}/m^2$). The surface-to-bulk transport rate increases to $k_2' \sim 2.5$ per pass as the annealing temperature decreases to 850 K (Figures 4 and 5), where the crystallite size (~250 nm, Table 1) is sufficiently large that there are no grain boundaries in the image in shown in Figure 4, while the dislocation density increases to $\sim 2.4 \times 10^{13}/m^2$ (Table 1). This clearly implicates the participation of dislocations in the transportation mechanism of sulfur into the copper bulk.

The sample that had been prepared at a lower temperature (500 K, Figure 6) contains smaller grains (~115 nm, Table 1), and has a higher dislocation density ($\sim 3.95 \times 10^{13}/m^2$). The sulfur penetrates still further into the bulk of the copper ($k_2' \sim$ 4 per pass, Table 1), in agreement with predictions from measurements of the surface-to-bulk transport kinetics (Figure 6, Inset). Thus, the surface-to-bulk transport rate of sulfur in crystalline regions of the copper sample scales with the dislocation density as evidenced by the plot in Figure 8, implying that strain-rate sensitivity depends on the dislocation

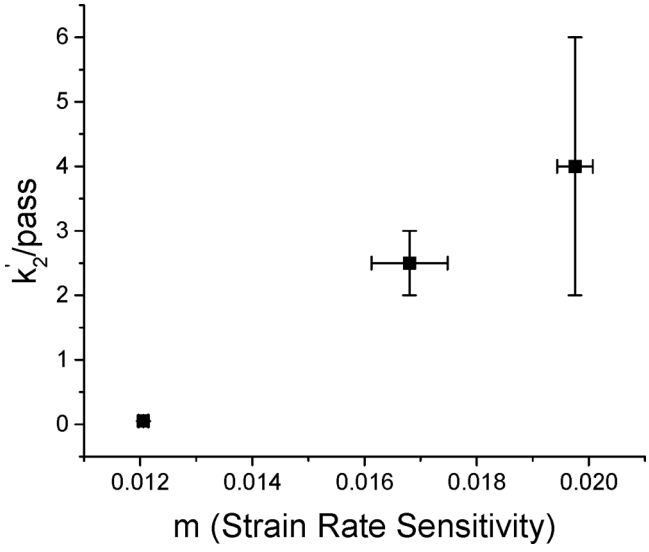

Figure 7. Plot of the rate constant for the shear-induced transport of sulfur into the subsurface region of copper, k_2', as a function of the strain-rate sensitivity for samples modified by heating the copper sample to various temperatures. The errors in the values of k_2' are the standard deviations of the fits to the data in Figure 1 and the errors in the strain rate sensitivities were obtained from the errors in the hardness values.

https://dx.doi.org/10.1021/acsami.0c18980
ACS Appl. Mater. Interfaces 2021, 13, 6785–6794

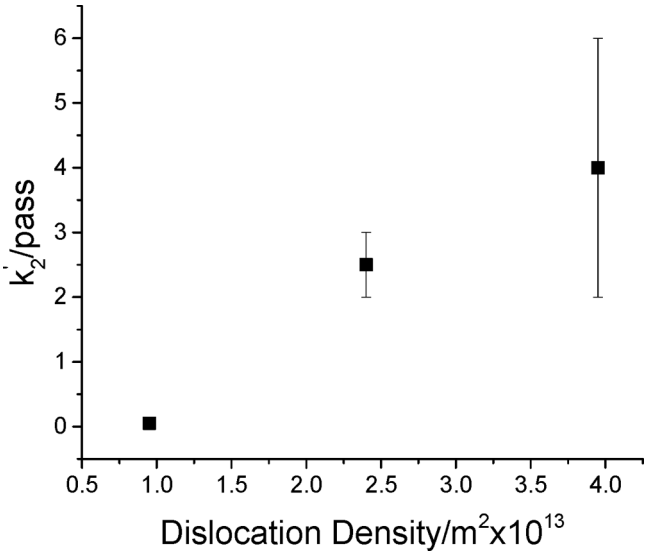

Figure 8. Plot of the rate constant for the shear-induced transport of sulfur into the subsurface region of copper, k_2', as a function of dislocation density for samples modified by heating the copper sample to various temperatures. The errors in the values of k_2' are the standard deviations of the fits to the data in Figure 1, and the errors in the dislocation densities were obtained from the errors of the hardness values.

density.[65] Note that the dislocation glide has been proposed as a mechanism for alloy formation during high-energy ball milling.[16−18]

However, in the case of a sample annealed at 500 K (Figure 6), some sulfur is detected even deeper in the copper in linear regions that coincide with the location of grain boundaries that are identified by electron microscopy (Figure S1d), suggesting that sulfur can also diffuse along grain boundaries. The linear regions are ∼20 nm wide, much wider than expected for grain boundaries in copper,[66] and may be due to the boundaries being tilted with respect to the incident electron beam. An alternative possibility is that because the width of the linear regions are relatively independent of depth into the substrate, the sulfur diffuses rapidly along grain boundaries when they are present but much more slowly via dislocations, where it diffuses away from the grain boundaries to form EDXS features that are ∼20 nm wide. These results suggest that both the presence of grain boundaries and dislocations can facilitate the surface-to-bulk transport of sulfur and the formation of a metastable phase.

It should be emphasized that the formation of nanostructured materials at the sliding interface by Kelvin−Helmholtz instabilities proposed by Rigney[35,36,67,68] is not directly captured by the analytical KR model used here. It should not, in principle, describe the experimental mixing behavior nor reproduce the kinetics and the strain-rate sensitivity dependence found experimentally, yet it does. However, finite-element simulations that have been performed using a nonlinear viscosity of copper analogous to the Herschel−Buckley model reveal deformation, material folding, and the occurrence of vortices while rubbing[6] that are reminiscent of Kelvin−Helmholtz instabilities.

CONCLUSIONS

The previously identified shear-induced transport of sulfur into the subsurface region of copper is investigated by modifying the material properties of copper by varying the annealing temperatures (500, 850, or 1020 K) during the vacuum cleaning procedure. The surface-to-bulk transport kinetics are modeled by an adaptation of a theory first proposed by Karthikeyan and Rigney that predicts that the distance that an adsorbed overlayer penetrates the bulk of the sample is proportional to the number of times that the sample was rubbed and that the rate should be proportional to the strain-rate sensitivity of the substrate. Previous work has verified the linear dependence of penetration depth on the number of rubbing cycles. It is found here, by measuring the hardness of the copper after it has been rubbed, that the temperature at which the copper sample was annealed during its preparation influences its hardness, and therefore its strain-rate sensitivity, m. This enables the second prediction of the Karthikeyan−Rigney model to be tested by measuring the surface-to-bulk transport rate by monitoring the loss of sulfur from the surface as a function of the number of times that the sample had been rubbed and showing that it does vary linearly with m, in accord with the theoretical prediction.

The mechanism for this process is investigated by preparing thin samples of the surface region of copper that had been annealed at 500, 850, or 1020 K during the cleaning procedure. Electron microscopy images of the samples indicate that larger crystallites were formed for samples that had been annealed at high temperatures, as expected. EDXS measurements as a function of depth into the sample revealed that the sulfur was highly localized for a sample that had been heated to 1020 K, penetrated a moderate distance (∼10 nm) into the surface for a sample that had been annealed to 850 K, and even deeper (∼65 nm) for a sample that had been heated to 500 K. For the samples that had been annealed to 1020 and 850 K, the crystallite size was sufficiently large that there were no grain boundaries in the analyzed region, while sulfur still penetrated into the bulk, implying the surface-to-bulk transport of sulfur is facilitated by the presence of dislocations in the copper. This observation is in accord with previous studies of mechanical mixing (alloy formation) by ball milling, which implicates a dislocation glide mechanism in the mixing.[16−18]

It was noted that the Karthikeyan and Rigney model does not specifically describe Kelvin−Helmholtz-type instabilities that would lead to intermixing near the surface and the transport of adsorbates into the subsurface region. However, more detailed finite-element calculations for copper using similar shear properties as the Karthikeyan and Rigney model by Pouryazdan et al.[6] identify flow features that resemble those formed by Kelvin−Helmholtz instabilities.

Finally, in the case of copper samples with smaller crystallites which have been cleaned by annealing at a lower temperature (∼500 K), additional sulfur is found deeper into the copper in locations that electron microscopy identifies as grain boundaries. It appears that rate of surface-to-bulk transport of sulfur into copper is facilitated by the presence both of dislocations and grain boundaries.

ASSOCIATED CONTENT

Supporting Information

The Supporting Information is available free of charge at https://pubs.acs.org/doi/10.1021/acsami.0c18980.

Figures S1 to S6, mechanical properties, and structure of annealed copper samples (PDF)

https://dx.doi.org/10.1021/acsami.0c18980
ACS Appl. Mater. Interfaces 2021, 13, 6785−6794

AUTHOR INFORMATION

Corresponding Author

Wilfred T. Tysoe − *Department of Chemistry and Laboratory for Surface Studies, University of Wisconsin-Milwaukee, Milwaukee, Wisconsin 53211, United States;* orcid.org/0000-0002-9295-448X; Email: wtt@uwm.edu

Authors

Resham Rana − *Department of Chemistry and Laboratory for Surface Studies, University of Wisconsin-Milwaukee, Milwaukee, Wisconsin 53211, United States*

Daniel Long − *Center for Integrated Nanotechnologies, Sandia National Laboratories, Albuquerque, New Mexico 87185, United States*

Paul Kotula − *Center for Integrated Nanotechnologies, Sandia National Laboratories, Albuquerque, New Mexico 87185, United States*

Yufu Xu − *Institute of Tribology, School of Mechanical Engineering, Hefei University of Technology, Hefei 230009, China;* orcid.org/0000-0002-1881-7583

Dustin Olson − *Department of Chemistry and Laboratory for Surface Studies, University of Wisconsin-Milwaukee, Milwaukee, Wisconsin 53211, United States*

Jules Galipaud − *Laboratoire de Tribologie et Dynamique des Systèmes, CNRS UMR5513, Ecole centrale de Lyon, F-69134 Ecully cedex, France*

Thierry LeMogne − *Laboratoire de Tribologie et Dynamique des Systèmes, CNRS UMR5513, Ecole centrale de Lyon, F-69134 Ecully cedex, France*

Complete contact information is available at: https://pubs.acs.org/10.1021/acsami.0c18980

Notes

The authors declare no competing financial interest.

ACKNOWLEDGMENTS

We gratefully acknowledge the Civil, Mechanical, and Manufacturing Innovation (CMMI) Division of the National Science Foundation under Grant CMMI-2020525 and 1634340 for support of this work. W.T.T. thanks LABEX Manutech-Sise (ANR-10-LABX-0075) of Université de Lyon, within the program "Investissements d'Avenir" (ANR-11-IDEX-0007) operated by the French National Research Agency (ANR) for travel support for a stay at the Laboratoire de Tribologie et Dynamique des Systèmes (LTDS). This work was performed, in part, at the Center for Integrated Nanotechnologies, an Office of Science User Facility operated for the U.S. Department of Energy (DOE) Office of Science. Sandia National Laboratories is a multimission laboratory managed and operated by National Technology and Engineering Solutions of Sandia, LLC, a wholly owned subsidiary of Honeywell International, Inc., for the U.S. DOE's National Nuclear Security Administration under contract DE-NA-0003525. The views expressed in the article do not necessarily represent the views of the U.S. DOE or the United States Government. We thank Dr. Katherine Jungjohann from Sandia National Laboratory for helping to organize this collaboration. We also thank Professors Lars Pastewka and David Rigney for very useful discussions.

REFERENCES

(1) Furlong, O. J.; Miller, B. P.; Tysoe, W. T. Shear-Induced Surface-to-Bulk Transport at Room Temperature in a Sliding Metal-Metal Interface. *Tribol. Lett.* **2011**, *41* (1), 257−261.

(2) Adams, H.; Miller, B. P.; Furlong, O. J.; Fantauzzi, M.; Navarra, G.; Rossi, A.; Xu, Y.; Kotvis, P. V.; Tysoe, W. T. Modeling Mechanochemical Reaction Mechanisms. *ACS Appl. Mater. Interfaces* **2017**, *9* (31), 26531−26538.

(3) Tan, D.; García, F. Main group mechanochemistry: from curiosity to established protocols. *Chem. Soc. Rev.* **2019**, *48* (8), 2274−2292.

(4) Fox, P. G. Mechanically initiated chemical reactions in solids. *J. Mater. Sci.* **1975**, *10* (2), 340−360.

(5) Meyers, M. A.; Mishra, A.; Benson, D. J. Mechanical properties of nanocrystalline materials. *Prog. Mater. Sci.* **2006**, *51* (4), 427−556.

(6) Pouryazdan, M.; Kaus, B. J. P.; Rack, A.; Ershov, A.; Hahn, H. Mixing instabilities during shearing of metals. *Nat. Commun.* **2017**, *8* (1), 1611.

(7) Suryanarayana, C. Mechanical alloying and milling. *Prog. Mater. Sci.* **2001**, *46* (1), 1−184.

(8) Vaidya, M.; Muralikrishna, G. M.; Murty, B. S. High-entropy alloys by mechanical alloying: A review. *J. Mater. Res.* **2019**, *34* (5), 664−686.

(9) Giannakoudakis, D. A.; Chatel, G.; Colmenares, J. C. Mechanochemical Forces as a Synthetic Tool for Zero- and One-Dimensional Titanium Oxide-Based Nano-photocatalysts. *Topics in Current Chemistry* **2020**, *378* (1), 2.

(10) Theophrastus, H. J. *Theophrastus's history of stones*; with an English version, and critical and philosophical notes, including the modern history of the gems, described by that author, and of many other of the native fossils; London, 1774.

(11) Faraday, M. M. J. K. *Chemical manipulation: being instructions to students in chemistry on the methods of performing experiments of demonstration or of research with accuracy and success*; Carey and Lea: Philadelphia, 1831.

(12) Kaupp, G. Waste-free synthesis and production all across chemistry with the benefit of self-assembled crystal packings. *J. Phys. Org. Chem.* **2008**, *21* (7−8), 630−643.

(13) Beyer, M. K.; Clausen-Schaumann, H. Mechanochemistry: The Mechanical Activation of Covalent Bonds. *Chem. Rev.* **2005**, *105* (8), 2921−2948.

(14) Thadhani, N. N. Shock-induced chemical reactions and synthesis of materials. *Prog. Mater. Sci.* **1993**, *37* (2), 117−226.

(15) James, S. L.; Adams, C. J.; Bolm, C.; Braga, D.; Collier, P.; Friscic, T.; Grepioni, F.; Harris, K. D. M.; Hyett, G.; Jones, W.; Krebs, A.; Mack, J.; Maini, L.; Orpen, A. G.; Parkin, I. P.; Shearouse, W. C.; Steed, J. W.; Waddell, D. C. Mechanochemistry: opportunities for new and cleaner synthesis. *Chem. Soc. Rev.* **2012**, *41* (1), 413−447.

(16) Bellon, P.; Averback, R. S. Nonequilibrium Roughening of Interfaces in Crystals under Shear - Application to Ball-Milling. *Phys. Rev. Lett.* **1995**, *74* (10), 1819−1822.

(17) Odunuga, S.; Li, Y.; Krasnochtchekov, P.; Bellon, P.; Averback, R. S. Forced chemical mixing in alloys driven by plastic deformation. *Phys. Rev. Lett.* **2005**, *95* (4), 045901.

(18) Ashkenazy, Y.; Vo, N. Q.; Schwen, D.; Averback, R. S.; Bellon, P. Shear induced chemical mixing in heterogeneous systems. *Acta Mater.* **2012**, *60* (3), 984−993.

(19) Panin, V.; Kolubaev, A.; Tarasov, S.; Popov, V. Subsurface layer formation during sliding friction. *Wear* **2001**, *249* (10−11), 860−867.

(20) Tarasov, S.; Rubtsov, V.; Kolubaev, A. Subsurface shear instability and nanostructuring of metals in sliding. *Wear* **2010**, *268* (1−2), 59−66.

(21) Moshkovich, A.; Perfilyev, V.; Lapsker, I.; Gorni, D.; Rapoport, L. The Effect of Grain Size on Stribeck Curve and Microstructure of Copper Under Friction in the Steady Friction State. *Tribol. Lett.* **2011**, *42* (1), 89−98.

(22) Moshkovich, A.; Perfilyev, V.; Lapsker, I.; Rapoport, L. Stribeck Curve Under Friction of Copper Samples in the Steady Friction State. *Tribol. Lett.* **2010**, *37* (3), 645−653.

(23) Mishra, A.; Kad, B. K.; Gregori, F.; Meyers, M. A. Microstructural evolution in copper subjected to severe plastic deformation: Experiments and analysis. *Acta Mater.* **2007**, *55* (1), 13−28.
(24) Gubicza, J.; Chinh, N. Q.; Csanádi, T.; Langdon, T. G.; Ungár, T. Microstructure and strength of severely deformed fcc metals. *Mater. Sci. Eng., A* **2007**, *462* (1−2), 86−90.
(25) Zhang, Y. S.; Han, Z.; Wang, K.; Lu, K. Friction and wear behaviors of nanocrystalline surface layer of pure copper. *Wear* **2006**, *260* (9−10), 942−948.
(26) Gao, F.; Furlong, O.; Kotvis, P. V.; Tysoe, W. T. Reaction of Tributyl Phosphite with Oxidized Iron: Surface and Tribological Chemistry. *Langmuir* **2004**, *20* (18), 7557−7568.
(27) Furlong, O. J.; Miller, B. P.; Kotvis, P.; Tysoe, W. T. Low-Temperature, Shear-Induced Tribofilm Formation from Dimethyl Disulfide on Copper. *ACS Appl. Mater. Interfaces* **2011**, *3* (3), 795−800.
(28) Furlong, O.; Miller, B.; Tysoe, W. T. Shear-induced boundary film formation from dialkyl sulfides on copper. *Wear* **2012**, *274*−*275* (0), 183−187.
(29) Adams, H.; Miller, B. P.; Kotvis, P. V.; Furlong, O. J.; Martini, A.; Tysoe, W. T. In Situ Measurements of Boundary Film Formation Pathways and Kinetics: Dimethyl and Diethyl Disulfide on Copper. *Tribol. Lett.* **2016**, *62* (1), 1−9.
(30) Varenberg, M.; Ryk, G.; Yakhnis, A.; Kligerman, Y.; Kondekar, N.; McDowell, M. T. Mechano-Chemical Surface Modification with Cu2S: Inducing Superior Lubricity. *Tribol. Lett.* **2016**, *64* (2), 28.
(31) Thomson, W. Hydrokinetic solutions and observations. *Philosophical Magazine Series 4* **1871**, *42* (281), 362−377.
(32) Helmholtz, H. v. Über discontinuierliche Flüssigkeits-Bewegungen. *Monatsberichte der Königlichen Preussische Akademie der Wissenschaften zu Berlin* **1868**, *23*, 13.
(33) Kim, H. J.; Kim, W. K.; Falk, M. L.; Rigney, D. A. MD simulations of microstructure evolution during high-velocity sliding between crystalline materials. *Tribol. Lett.* **2007**, *28* (3), 299−306.
(34) Emge, A.; Karthikeyan, S.; Kim, H. J.; Rigney, D. A. The effect of sliding velocity on the tribological behavior of copper. *Wear* **2007**, *263*, 614−618.
(35) Kim, H. J.; Karthikeyan, S.; Rigney, D. A simulation study of the mixing, atomic flow and velocity profiles of crystalline materials during sliding. *Wear* **2009**, *267* (5−8), 1130−1136.
(36) Karthikeyan, S.; Agrawal, A.; Rigney, D. A. Molecular dynamics simulations of sliding in an Fe-Cu tribopair system. *Wear* **2009**, *267* (5−8), 1166−1176.
(37) Emge, A.; Karthikeyan, S.; Rigney, D. A. The effects of sliding velocity and sliding time on nanocrystalline tribolayer development and properties in copper. *Wear* **2009**, *267* (1−4), 562−567.
(38) Rigney, D. A.; Karthikeyan, S. The Evolution of Tribomaterial During Sliding: A Brief Introduction. *Tribol. Lett.* **2010**, *39* (1), 3−7.
(39) Argibay, N.; Chandross, M.; Cheng, S.; Michael, J. R. Linking microstructural evolution and macro-scale friction behavior in metals. *J. Mater. Sci.* **2017**, *52* (5), 2780−2799.
(40) Gola, A.; Schwaiger, R.; Gumbsch, P.; Pastewka, L. Pattern formation during deformation of metallic nanolaminates. *Physical Review Materials* **2020**, *4* (1), 013603.
(41) Karthikeyan, S.; Kim, H. J.; Rigney, D. A. Velocity and Strain-Rate Profiles in Materials Subjected to Unlubricated Sliding. *Phys. Rev. Lett.* **2005**, *95* (10), 106001.
(42) Herschel, W.; Bulkley, R. Konsistenzmessungen von Gummi-Benzollösungen. *Colloid Polym. Sci.* **1926**, *39* (4), 291−300.
(43) Zhu, T.; Li, J.; Samanta, A.; Kim, H. G.; Suresh, S. Interfacial plasticity governs strain rate sensitivity and ductility in nanostructured metals. *Proc. Natl. Acad. Sci. U. S. A.* **2007**, *104* (9), 3031−3036.
(44) Shen, Y. F.; Lu, L.; Dao, M.; Suresh, S. Strain rate sensitivity of Cu with nanoscale twins. *Scr. Mater.* **2006**, *55* (4), 319−322.
(45) Mishra, A.; Martin, M.; Thadhani, N. N.; Kad, B. K.; Kenik, E. A.; Meyers, M. A. High-strain-rate response of ultra-fine-grained copper. *Acta Mater.* **2008**, *56* (12), 2770−2783.
(46) Schwaiger, R.; Moser, B.; Dao, M.; Chollacoop, N.; Suresh, S. Some critical experiments on the strain-rate sensitivity of nanocrystalline nickel. *Acta Mater.* **2003**, *51* (17), 5159−5172.
(47) Höppel, H. W.; May, J.; Göken, M. Enhanced Strength and Ductility in Ultrafine-Grained Aluminium Produced by Accumulative Roll Bonding. *Adv. Eng. Mater.* **2004**, *6* (9), 781−784.
(48) Gray, G. T.; Lowe, T. C.; Cady, C. M.; Valiev, R. Z.; Aleksandrov, I. V. Influence of strain rate & temperature on the mechanical response of ultrafine-grained Cu, Ni, and Al-4Cu-0.5Zr. *Nanostruct. Mater.* **1997**, *9* (9), 477−480.
(49) Petch, N. J. The Cleavage Strength of Polycrystals. *Journal of the Iron and Steel Institute* **1953**, *174*, 25−28.
(50) Hall, E. O. The Deformation and Ageing of Mild Steel: III Discussion of Results. *Proc. Phys. Soc., London, Sect. B* **1951**, *64* (9), 747−753.
(51) Gao, F.; Furlong, O.; Kotvis, P. V.; Tysoe, W. T. Pressure dependence of shear strengths of thin films on metal surfaces measured in ultrahigh vacuum. *Tribol. Lett.* **2008**, *31* (2), 99−106.
(52) Olson, D.; Gao, H.; Tang, C.; Tysoe, W. T.; Martini, A. Pressure dependence of the interfacial structure of potassium chloride films on iron. *Thin Solid Films* **2015**, *593*, 150−157.
(53) Lu, L.; Schwaiger, R.; Shan, Z. W.; Dao, M.; Lu, K.; Suresh, S. Nano-sized twins induce high rate sensitivity of flow stress in pure copper. *Acta Mater.* **2005**, *53* (7), 2169−2179.
(54) Furlong, O.; Miller, B.; Tysoe, W. Shear-Induced Surface-to-Bulk Transport at Room Temperature in a Sliding Metal−Metal Interface. *Tribol. Lett.* **2011**, *41* (1), 257−261.
(55) Miller, B.; Furlong, O.; Tysoe, W. The Kinetics of Shear-Induced Boundary Film Formation from Dimethyl Disulfide on Copper. *Tribol. Lett.* **2013**, *49* (1), 39−46.
(56) Chen, J.; Lu, L.; Lu, K. Hardness and strain rate sensitivity of nanocrystalline Cu. *Scr. Mater.* **2006**, *54* (11), 1913−1918.
(57) Furlong, O. J.; Miller, B. P.; Li, Z.; Walker, J.; Burkholder, L.; Tysoe, W. T. The Surface Chemistry of Dimethyl Disulfide on Copper†. *Langmuir* **2010**, *26* (21), 16375−16380.
(58) Adams, H. L.; Garvey, M. T.; Ramasamy, U. S.; Ye, Z.; Martini, A.; Tysoe, W. T. Shear-Induced Mechanochemistry: Pushing Molecules Around. *J. Phys. Chem. C* **2015**, *119* (13), 7115−7123.
(59) Kotula, P. G.; Keenan, M. R.; Michael, J. R. Automated Analysis of SEM X-Ray Spectral Images: A Powerful New Microanalysis Tool. *Microsc. Microanal.* **2003**, *9* (1), 1−17.
(60) Kotula, P. G.; Keenan, M. R. Application of Multivariate Statistical Analysis to STEM X-ray Spectral Images: Interfacial Analysis in Microelectronics. *Microsc. Microanal.* **2006**, *12* (6), 538−544.
(61) Mishin, Y.; Herzig, C.; Bernardini, J.; Gust, W. Grain boundary diffusion: fundamentals to recent developments. *Int. Mater. Rev.* **1997**, *42* (4), 155−178.
(62) Moya, F.; Moya-Gontier, G. E.; Cabane-Brouty, F. Sulphur Diffusion in Copper: Departure from the Arrhenius Plot. *Phys. Status Solidi B* **1969**, *35* (2), 893−901.
(63) Ladet, J.; Aufray, B.; Maya, F. Sulphur diffusion in silver and copper single crystals. *Met. Sci.* **1978**, *12* (4), 195−197.
(64) Malygin, G. A. Analysis of the strain-rate sensitivity of flow stresses in nanocrystalline FCC and BCC metals. *Phys. Solid State* **2007**, *49* (12), 2266−2273.
(65) Rodríguez-Martínez, J. A.; Rodríguez-Millán, M.; Rusinek, A.; Arias, A. A dislocation-based constitutive description for modeling the behavior of FCC metals within wide ranges of strain rate and temperature. *Mech. Mater.* **2011**, *43* (12), 901−912.
(66) Islamgaliev, R. K.; Pekala, K.; Pekala, M.; Valiev, R. Z. The determination of the grain boundary width of ultrafine grained copper and nickel from electrical resistivity measurements. *Physica Status Solidi a-Applications and Materials Science* **1997**, *162* (2), 559−566.
(67) Kim, H.; Kim, W.; Falk, M.; Rigney, D. MD Simulations of Microstructure Evolution during High-Velocity Sliding between Crystalline Materials. *Tribol. Lett.* **2007**, *28* (3), 299−306.
(68) Rigney, D.; Karthikeyan, S. The Evolution of Tribomaterial During Sliding: A Brief Introduction. *Tribol. Lett.* **2010**, *39* (1), 3−7.

https://dx.doi.org/10.1021/acsami.0c18980
ACS Appl. Mater. Interfaces 2021, 13, 6785−6794